Velocity Profiles in the Solar Corona from Multi-Instrument Observations

E. Quémerais, R. Lallement, D. Koutroumpa

Service d'Aéronomie, Verrières le Buisson, France

and

P. Lamy

Laboratoire d'Astrophysique de Marseille, Marseille, France

ABSTRACT

We present a method to derive outflow velocities in the solar corona using different data sets including solar wind mass flux coming from the SWAN/SOHO instrument, electron density values from LASCO-C2 and interplanetary solar wind velocities derived from ground-based Interplanetary Scintillation Observations (IPS).

In a first step, we combine the LASCO electron densities at 6 $R_\odot$ and the IPS velocities, and compare the product to the SWAN mass fluxes. It is found that this product represents the actual mass flux at 6 $R_\odot$ for the fast wind, but not for the slow wind. In regions dominated by the slow wind, the fluxes derived from SWAN are systematically smaller. This is interpreted as a proof that the fast solar wind has reached its terminal velocity at $\sim$ 6 $R_\odot$ and expands with constant velocity beyond this distance. On the contrary, the slow solar wind has reached only half of its terminal value and is thus accelerated further out.

In a second step, we combine the LASCO-C2 density profiles and the SWAN flux data to derive velocity profiles in the corona between 2.5 and 6 $R_\odot$. Such profiles can be used to test models of the acceleration mechanism of the fast solar wind.

Subject headings: The Sun — The Corona

1. Introduction

There is no consensus on the mechanisms of energy deposition and solar wind acceleration in the low corona, especially in the fast wind, although major results have been obtained

with the SOHO instruments. In particular, UV spectroscopy has led to the discovery of high ion temperatures and significantly lower electronic temperatures in coronal holes, as well as strong ion temperature anisotropies (e.g., Kohl et al., 2006; David et al., 1998). A number of models have been developed to reproduce these properties, with damping of high frequency waves and ion cyclotron heating as favoured mechanisms. Because one of the strong difficulties in modeling the solar wind expansion is linked to the heat flux in regions which are not collisional enough for classical transport theory to be valid, kinetic models have also been developed. These models are able to reproduce the acceleration by velocity filtration (e.g., Zouganelis et al., 2005), although they do not reproduce the published temperature anisotropies. Since all different classes of models predict different velocity profiles, accurate measurements of the solar wind flow speed in the acceleration region are required to decide which models are correct.

One of the methods to obtain the flow speed profile in the acceleration region relies on the measured coronal density profile as well as the expanding geometry. The velocity profile is simply obtained from the application of the continuity equation, assuming a value for the particle flux coming from the observed region. The flux is inferred from in situ or remote sensing measurements. Munro and Jackson (1977) pioneered this method using Skylab white-light coronographic images of polar coronal holes. Assuming that the solar flux is roughly constant at all latitudes, they used its average ecliptic value. They concluded that there is a substantial energy addition in the low corona, and that the flow accelerates to supersonic speed within 2-3$R_{\odot}$.

Later on, the analysis of solar backscattered Lyman-alpha radiation led to the derivation of a significantly lower mass flux in the polar regions (Kumar and Broadfoot, 1979; Lallement et al., 1985a). It was shown that the requirement for a non-thermal mechanism is strongly dependent on the density profile and on the out-of-ecliptic mass flux (Lallement et al., 1985b). However, our knowledge of the solar wind conditions outside of the ecliptic plane is very limited as most of the in situ studies of the solar wind are based on data obtained in the ecliptic plane. Because of the small angle (7 degrees) between the ecliptic plane and the solar equatorial plane, this means that most of our knowledge on the solar wind concerns the wind which originates close to the solar equator.

In this article, we present a new approach to the determination of velocity profiles in the solar corona. The steps are the following,

- The velocity at large distance from the Sun is obtained from Interplanetary Scintillation data (Kojima et al., 1998).

- Using the SWAN interplanetary Lyman α data, we can derive the ionization rate

of hydrogen at 1 AU. After removal of the contributions from photo-ionization and electron impact ionization, we obtain the ionization rate due to charge exchange with the solar wind protons.

- Using the value of the charge exchange cross section, which depends on solar wind velocity, we compute the solar wind flux.

- Assuming radial expansion, we derive the solar wind velocity profile from the values of coronal density and solar wind mass flux. The assumption of radial expansion is not necessary. We could introduce a correction term for non-radial expansion.

- The previous relation is then applied to the density profiles obtained from the LASCO-C2 polarized white light images, between $2.5R_\odot$ and $6R_\odot$.

In what follows, we concentrate on a test period from 1996 to 1997 corresponding to a minimum in the solar activity cycle. We briely present the results of Quémerais et al. (2006) for this period. We then show how mean values of density and velocity can be derived. In the last paragraph, we show how this information can be combined with density profiles in the solar corona to give information on velocity profiles.

In our conclusion, we discuss the velocity profiles found in the corona and how they relate to fast wind or slow wind conditions. These results are relevant to studies of the mechanism of the solar wind acceleration.

2. Method of Analysis

The Lyman α background is due to the backscatter of solar Lyman α photons by hydrogen atoms present in the interplanetary medium. This UV emission was first identified by instruments on board the OGO-8 spacecraft (Bertaux and Blamont, 1971; Thomas and Krassa, 1971). The hydrogen atoms of the local insterstellar cloud can get very close to the Sun because of the motion of the solar system relative to the local cloud. In the vicinity of the sun, the hydrogen atoms are ionized by charge exchange with solar wind protons or photo-ionized by solar EUV radiation or, with a lesser probability, ionized by collision with hot solar wind electrons.

In the inner heliosphere the spatial pattern of the full-sky Lyman α background is carved by the ionizing fluxes from the Sun (Jozelyn and Holzer, 1975; Kumar and Broadfoot, 1979). Once a hydrogen atom loses its electron, it cannot backscatter Lyman α photons anymore. This creates a hole in the sky pattern. Areas of the sky where ionization is more effective

appear dimmer at Lyman α because there are less hydrogen atoms which can backscatter solar Lyman α photons. The most effective ionization process, roughly 4 times out of 5, is charge exchange with solar wind protons. Even in that case, the hydrogen atom is lost because the hydrogen atom which captured the electron has the velocity of the solar wind proton, i.e. at least a few hundred km/s. The illuminating solar Lyman α line is roughly 1 Angström wide. In terms of Doppler shift, this corresponds to 150 km/s. This means that a hydrogen atom with a velocity larger than 150 km/s is blind to solar Lyman α photons and this results in a loss of hydrogen atoms able to backscatter the solar atoms exactly as in the case of photo-ionization.

Quémerais et al. (2006) published an analysis of the full-sky background maps obtained with SWAN/SOHO between 1996 and 2005. The maps were used to derive the hydrogen ionization rate at 1 AU at all heliographic latitudes. We will use these values to derive the solar mass flux and its latitudinal dependence. The ionization rate of hydrogen is the sum of three terms, the photo-ionization rate, the charge exchange ionization rate, and the electron impact ionization rate. Photo-ionization and charge exchange have a radial dependence like the inverse of the square of the distance to the sun. The photon flux and the solar particle flux have approximately the same radial variation. The electron impact ionization rate also varies with the solar wind electron temperature which is not constant with distance to the sun so its total radial dependence is not like the inverse of the square of the distance to the sun. Using the solar wind electron distribution values obtained by the WIND/waves experiment (Issautier et al., 2004) we have computed the absolute value of the electron impact ionization rate at 1 AU between 1994 and 2001. We have found values between 10^{-8} s^{-1} at solar minimum and a few 10^{-8} s^{-1} at solar maximum. The total ionization rate found by Quémerais et al. (2006) varies between 6 10^{-7} s^{-1} and 1.2 10^{-6} s^{-1}, i.e. almost two orders of magnitude larger. Then, because electron impact ionization is small compared to the two other sources of ionization, we will neglect it and assume that the total ionization rate of hydrogen varies like the inverse of the square of the distance to the sun.

The total ionization rate β_{tot} at 1 AU can be written as

$$\beta_{tot} = \beta_{exc} + \beta_{phot} + \beta_{eii} = \sigma_{exc}(v_{sw}) \cdot v_{sw} \cdot N_{sw} + \beta_{phot} + \beta_{eii} \tag{1}$$

In the previous equation, we neglect the velocity of the hydrogen atom before the solar wind speed v_{sw}. The charge exchange cross section variation with velocity $\sigma_{exc}(v_{sw})$ is given by

$$\sigma_{exc}(v_{sw}) \cdot v_{sw} = \frac{\beta_{tot} - (\beta_{phot} + \beta_{eii})}{N_{sw}} \tag{2}$$

Equation 2 can be used to derive the solar wind mass flux from the knowledge of β_{exc} and the density of the solar wind. In the range 0-1200 km/s the product $\sigma_{exc}(v_{sw}) \cdot v_{sw}$ is a monotonic function of the velocity v_{sw}, and can easily be inverted. The charge exchange ionization rate is obtained from the SWAN data analysis once a value for photo-ionization and electron impact ionization has been removed.

The velocity profile $V(R)$ is simply derived using the flux conservation which can be written as follows, where R is the distance from the Sun center (in $R_\odot$), and R_o is 1 AU,

$$N(R) \cdot V(R) \cdot R^2 = N_o \cdot V_o \cdot R_o^2 \tag{3}$$

In that case the the velocity profile is given by

$$V(R) = \frac{\beta_{exc}}{\sigma_{exc}(V_o)} \frac{R_o^2}{R^2} \frac{1}{N(R)} \tag{4}$$

This formalism will be used in the following sections.

3. Data Sets

3.1. Solar Wind Mass Flux: SWAN data

The Solar Wind ANisotropy (SWAN) instrument on-board the SOHO spacecraft was developed in a collaboration between Service d'Aéronomie (Verrières le Buisson, France) and the Finnish Meteorological Institute (Helsinki, Finland) (Bertaux et al., 1995). Its main purpose is to study anisotropies in the solar wind mass flux and their effect on the interplanetary background (Bertaux et al., 1997). Thanks to the exceptional longevity of the SOHO mission, the data obtained by this instrument almost cover a complete 11-year solar activity cycle.

The most recent analysis of the SWAN data pertaining to the determination of the ionizing fluxes from the Sun was published by Quémerais et al. (2006). In this study, the authors have determined the absolute value of the ionization rate of hydrogen at 1 AU as a function of heliographic latitude and its variations with heliographic latitude. Their analysis covers the period from 1996 to 2005, i.e. almost a complete solar cycle. The Hydrogen ionization rate is related to the solar wind mass flux as shown in equation (2). After correction for solar EUV photo-ionization and the variation of the charge exchange cross-section with solar wind bulk velocity, the SWAN data give monthly averages of the solar wind mass flux at all latitudes between 1996 and 2005.

3.2.   Solar Wind Density: LASCO data

In principle, the solar wind number density at 1 AU can be estimated from in situ measurements performed by numerous spacecrafts proeminently restricted to the ecliptic plane. However results from the Ulysses spacecraft have demonstrated that the density at higher latitudes can be very different from that in the ecliptic (Phillips et al., 1995).

We have therefore relied on the LASCO-C2 white light images to obtain an estimate of the solar wind density at all latitudes. The LASCO-C2 polarized radiance images pB are routinely generated from the daily polarization sequences consisting a set of three polarized images taken through the orange filter (540-640 nm) and polarizers oriented at $60^o, 0^o$ and -60°. Quémerais and Lamy (2002) have developed a method to invert these images and to produce two-dimensional electron density maps of the solar corona. Compared to our past studies (see also Lamy et al., 1997; LLebaria et al., 1999; Lamy et al., 2002), the maps used for this present studies have benefited from refined corrections which successfully remove the instrumental polarization. The values at $6R_\odot$ from the center of the Sun have been extracted at all heliographic latitudes. We have then computed a monthly average from the daily maps to obtain values with the same sampling as the ionization rate derived from the SWAN data. We discuss below in which cases the density at $6R_\odot$ can be simply extrapolated at 1 AU.

3.3.   Solar Wind Terminal Velocity: IPS data

As one can see from a quick perusing through the catalog of the omniweb database, various spacecraft have measured the solar wind velocity in the ecliptic plane, but only a few measurements are available at mid and high heliographic latitude. Here we have used the solar wind velocity estimates obtained from Interplanetary Scintillation data (IPS) (Kojima and Kakinuma, 1990). These velocity values are derived from the analysis of scintillations of radio-emissions from compact radio sources (Kojima et al., 1998). Because the distribution of radio sources in the sky is not uniform, the sampling of these measurements is not either. These authors have found that the solar wind speed is roughly constant beyond 0.1 AU from the sun which means that the acceleration occurs before. Here we have averaged the velocity values beyond 0.1 AU from the sun as a function of the heliographic latitude from which the wind originates. Those averages were made on a monthly basis. It should be noted also that there is a 4 month data gap every year due to the weather conditions which prevent the ground-based radio observations.

4. Results

4.1. Computation of H Ionization Rates

The first step in our analysis is to check whether SWAN results are compatible with the LASCO density values, the IPS velocity estimates and the assumption that the IPS velocity is reached at the outer edge of LASCO-C2. To do that, we compute the charge exchange ionization rate at one AU β_{exc} where the velocity is derived from the IPS data and the density is equal to the value found from the LASCO images with a radial scaling coefficient. This coefficient expresses the relationship between the density measured by LASCO at $6R_\odot$ and the density at 1 AU. For a radial expansion, the product $N \cdot V \cdot r^2$ is conserved. If the acceleration is finished, then the velocity is constant and the density varies like $1/r^2$.

Figure 1 shows the paramaters and calculations obtained in April-May 1996. The top left panel shows the LASCO-C2 average density at $6R_\odot$ as a function of heliographic latitude. There is a strong enhancement in the equatorial band. The top-right panel shows the IPS mean velocity as a function of heliographic latitude for the same period. The bottom-left panel shows the ionization rate of hydrogen at 1 AU. The diamonds linked by a dotted line correspond to the SWAN data. The solid line corresponds to the value derived from the scaled LASCO density and the IPS velocity data. The computed value represents only ionization through charge exchange. The bottom-right panel shows the difference of the two curves shown in the bottom-left panel. In this plot, we see two different regimes. In the equatorial band, the computed charge exchange rate is systematically larger than the SWAN total ionization rate. This means that the velocity between $6R_\odot$ and 1 AU is not constant and that the radially scaled density is overestimated. This also implies that the velocity at 1 AU is larger than the velocity at $6R_\odot$ which means that in the equatorial band, the solar wind has not completed its acceleration. Outside of the equatorial band, the SWAN ionization rates are systematically larger than the computed charge exchange ionization rate. This is consistent with the fact that in this region the solar wind has reached its terminal velocity and that the density simply scales like $1/r^2$ with solar distance. The difference between the two values can be attributed to the sum of photo-ionization and electron impact ionization.

Figure 2 shows a very similar picture. The values shown here are for April-May 1997. Once again, the equatorial belt data suggest that the wind is not completely accelerated while at higher latitudes the ionization rate values agree well.

Figure 3 shows the difference between the SWAN total ionization rate β_{tot} and the charge exchange ionization rate β_{exc} computed from LASCO and IPS data as a function of the IPS solar wind velocity. All monthly values for different heliographic latitudes have been used. The data are averaged over intervals of 10 degrees in latitude. Two patterns

appear clearly. For velocities larger than 500 km/s, the quantity $\beta_{tot} - \beta_{exc}$ is positive. Its mean value is equal $(5.3 \pm 2.3) \times 10^{-8}$ s^{-1}. This is consistent with the fact that for the fast wind conditions (here faster than 500 km/s), the acceleration is completed at $6R_\odot$ and that the solar wind density at 1 AU is correctly derived from the LASCO value scaled by $1/r^2$. In that case, the difference between total ionization rate and charge exchange ionization rate is equal to the sum of hydrogen photo-ionization rate and electron impact ionization rate. The value of $(5.3 \pm 2.3) \times 10^{-8}$ s^{-1} found here is compatible with previously estimated values. For example hydrogen photo-ionization rate estimates for solar minimum conditions range between 5×10^{-8} s^{-1} (Rucinski and Fahr, 1991) to 10^{-7} s^{-1} (Ogawa et al., 1995). We estimated electron impact ionization rates for hydrogen using the WIND/WAVES data (Issautier et al., 2005) and found values around 10^{-8} s^{-1} close to solar minimum.

When the IPS velocity value is lower than 500 km/s, we find that the quantity $\beta_{tot} - \beta_{exc}$ is negative. As mentioned above, the flux conservation from $r_i = 6R_\odot$ to 1 AU also contains a ratio $V(r_i)/V(1AU)$. This suggests that for slow solar wind conditions, the solar wind has not yet reached its terminal velocity, and that the ratio $V(r_i)/V(1AU)$ is smaller than one, assuming a radial outflow as defined in equation (3).

Here we find a clear dichotomy between fast solar wind regions at high latitude and slow solar wind regions near the equatorial region.

4.2. Velocity Profiles in the Corona

Figure 4 shows the LASCO-C2 electronic density radial profiles in spring 1996 averaged over the same period as the SWAN data. This results in very regular curves where most transient effects like CME's have been smoothed out. The two solid lines show the East limb and West limb density profiles. The dashed line shows the North pole density profile and the dotted line shows the south pole density profile. Within 2.5 $R_\odot$ of the Sun, the data are contaminated by the instrument scatterred light and the uncertainty is large. The profiles can only be used with confidence between 2.5 $R_\odot$ and 6 $R_\odot$. We see that the pole profiles have densities which are 10 times lower than the equatorial values.

Figure 5 displays the velocity profiles derived from the densities in Figure 4 using equation (4). The flux scaling factor $\frac{\beta_{exc}}{\sigma_{exc}(V_o)}$ is derived from the SWAN data of the same date. The solid line shows the radial dependence of the solar wind as a function of distance for the average of North and South poles. On the right hand we have plotted the corresponding IPS value around 600 km/s. The dotted line shows the individual profiles derived for the north and south poles. They are very similar to the average profile. From these profiles, we see

that the solar wind goes from about 200 km/s at $2.5R_{\odot}$ up to ~ 600 km/s at $4.5R_{\odot}$. After a distance of $5R_{\odot}$, the increase of solar wind velocity is less pronounced and acceleration is essentially finished at $6R_{\odot}$.

The dashed line shows the profile derived using the average of the two equatorial density profiles shown in figure 4. Once again the flux scaling ratio is derived from the SWAN equatorial data for the same period. The corresponding IPS velocity value is shown on the right hand part of the plot and has a value close to 400 km/s. We see that for the slow wind, the mean velocity at $6R_{\odot}$ is only 200 km/s, i.e. half of the terminal velocity. This result is limited by the assumption of radial expansion which is implicit in equation (4). Although this assumption is quite justified for a polar coronal hole above $5R_{\odot}$ or $6R_{\odot}$, this may not be the case for the equatorial slow wind. In that case a correction term should be applied to take into account the non-radial part of the slow wind expansion. Furthermore, this profile concerns an average of many transient phenomena which may have had very different individual velocity profiles.

5. Comparison with other works

The present work provides time-averaged velocity profiles at all latitudes. Coronal flow velocities have been obtained in specific regions and at specific times in different ways. The outflow velocity has been inferred from analyses of the Doppler dimming of the intensities of the OVI 1032Å, 1037 Å , HI Lα 1216Å lines, using the UVCS on board SOHO. In particular, Strachan et al. (2000) derived the latitudinal dependence of O5+ outflow velocities between 1.75 $R_{\odot}$ and 2.75 $R_{\odot}$. Gabriel et al. (2005) derive an outflow velocity of 150-200 km/ at 2.5 R_s in polar plumes. Kohl et al. (1998), Cranmer et al. (1999) and Antonucci et al. (2000) show that in a polar hole, the fast wind speed reaches 300-400 km/s near $3R_{\odot}$. On the other hand, Raymond et al. use UVCS observations of a sun-grazing comet at $6.8R_{\odot}$ and derive an outflow velocity smaller than 640 km/s in an high speed wind region. They argued that only 50% to 75% of the 1 AU proton energy is reached at $6.8R_{\odot}$ and, that an additional energy deposition is at work beyond this distance.

Above streamers, Strachan et al. (2002) derived a null velocity up to $3.5R_{\odot}$ and an abrupt acceleration to 90 km/s at $5R_{\odot}$ along the streamer axis, while along the streamer legs the velocity has already reached 100 km/s at $2.33R_{\odot}$. Based on expanding features, Sheeley et al. (1997) estimated the acceleration of the slow wind above streamers and found it compatible with a Parker-type isothermal expansion with values ranging from 150 to 300 km/s between $5R_{\odot}$ and $25R_{\odot}$.

In the open field/fast wind regions, the geometry is extremely simple and the comparison between previous localised measurements and the monthly-averaged SWAN/LASCO/IPS results can be directly performed. Indeed, there is a quite good agreement with SUMER and UVCS results between $2R_{\odot}$ and $3R_{\odot}$. The agreement suggests that the fast wind acceleration is rather homogeneous and constant with time. Note that the flow speed we derived is however above the maximum speed at $6.8R_{\odot}$ deduced from the Sun-grazing comet.

For the slow wind the comparison is not so easy because it originates in and around closed-field regions with a more complicated geometry. It has been shown by Strachan et al. (2002) that the profiles vary strongly from the streamer axis to the legs. Since the streamers vary in angle, latitude, and shape more work is needed to interpret the average profile.

6. Conclusion

In this article, we have shown how we can retrieve velocity profiles in the corona between $2.5R_{\odot}$ and $6R_{\odot}$.

This analysis has been applied to data from 1996 and 1997. We have used monthly averages because the SWAN inversion technique is based on data covering at least one solar rotation. We have found that during solar minimum, there is a strong difference between the velocity profiles derived for the polar and the equatorial regions of the Sun. The polar regions show a fast solar wind with lower density at 1 AU while the equatorial regions are the source of the slow solar wind with increased density. This features was already well known from analysis of the Interplanetary Scintillation data (Kojima and Kakinuma, 1990) or the Ulysses fast latitudinal scan of 1994 (Phillips et al., 1995).

Using the LASCO density values derived at $6R_{\odot}$, we have been able to show that the fast wind has a radial expansion with constant velocity beyond $6R_{\odot}$. This confirms the idea that the fast solar wind is accelerated at low altitudes in the corona and that it has already reached its terminal velocity at $6R_{\odot}$. This also means that the density ratio between $6R_{\odot}$ and 1 AU is simply scaled by the ratio of the square of the distance to the Sun (equation 3, where $V(R) = V_o$ and R = 6 $R_{\odot}$). On a side note, we can also mention that in this case, a combination of the SWAN flux data with the LASCO density values can be used to derive the velocity value at 1 AU without the need of the information given by the IPS analysis.

The slow wind originating from equatorial regions of the Sun shows a different behaviour. First, we have seen that the density ratio between $6R_{\odot}$ and 1 AU is not simply equal to the ratio of the square of the distance to the sun. This is shown by computing the flux using the density and the IPS velocity and comparing to the SWAN value. We see that the

SWAN value is always smaller which means that the velocity ratio between the outer edge of LASCO-C2 and 1 AU, $V(6R_\odot)/V_o$, is smaller than one.

As shown in Figure 3, the threshold between fast and slow winds is ~ 500 km/s. Below that threshold, the wind has not reached its terminal velocity at $6R_\odot$ while it has reached its terminal velocity at $6R_\odot$ for values larger than 500 km/s. The velocity profile for the slow wind may be different from the one we have produced if the expansion factor is not purely radial. This may be true at lower altitudes in the corona.

Finally, our velocity profiles provide a test of the models of solar wind acceleration to reveal which mechanisms are really effective. In future developments of this work, we will extend this study to all periods of solar activity. The corresponding SWAN data used to derive the solar wind flux at 1 AU have already been analysed by Quémerais et al. (2006). This will allow us to study the variation of the acceleration profile with solar activity.

REFERENCES

Ajello J.M, Stewart A.I., Thomas G.E. & Graps A. 1987; Astrophysical Journal, 317, 964

Baranov V. B. & Malama Y. G., 1993; J. Geophys. Res., 98, 15157

Bertaux J.L., Blamont J.E., 1971; Astronomy & Astrophysics, 11, 200.

Bertaux J. L., Lallement R., Kurt V.G., Mironova E.N.; 1985; Astronomy & Astrophysics, 150, 82.

Bertaux, J. L.; Kyrölä, E.; Quémerais, E.; R.; Lallement, R.; Schmidt, W.; et al., 1995; Solar Physics, v. 162, p. 403-439.

Bertaux, J. L.; Lallement, R.; Quémerais, E., 1996; Space Science Reviews, v. 78, Issue 1/2, p. 317-328.

Bertaux, J. L.; Quémerais, E.; Lallement, R.; Kyroela, E.; Schmidt, W.; Summanen, T.; Goutail, J. P.; Berthe, M.; Costa, J.; Holzer, T., 1997; Solar Physics, v. 175, Issue 2, p. 737-770.

Cranmer, S. R., et al. 1999, ApJ, 511, 481

David, C., Gabriel, A. H., Bely-Dubau, F., Fludra, A., Lemaire, P., & Wilhelm, K. 1998, A&A, 336, L90.

Gabriel, A. H., Abbo, L., Bely-Dubau, F., Llebaria, A., & Antonucci, E. 2005, ApJ, 635, L185

Issautier, K.; Perche, C.; Hoang, S.; Lacombe, C.; Maksimovic, M.; Bougeret, J.-L.; Salem, C.; 2005; Advances in Space Research, Volume 35, Issue 12, p. 2141-2146.

Izmodenov, Vladislav V.; Gruntman, Mike; Malama, Yury G., 2001; Journal of Geophysical Research, Volume 106, Issue A6, p. 10681-10690.

Joselyn, J. A.; Holzer, T. E., 1975, Journal of Geophysical Research, vol. 80, Mar. 1, 1975, p. 903-907

Kohl, J. L., et al. 1998, ApJ, 501, L127

Kojima,M. and T. Kakinuma, Space Sci. Rev., 53, 173-222, 1990.

Kojima, M.; Tokumaru, M.; Watanabe, H.; Yokobe, A.; Asai, K.; Jackson, B. V.; Hick, P. L.; 1998; Journal of Geophysical Research, vol. 103, p. 1981

Kohl, J. L., Noci, G., Cranmer, S. R., & Raymond, J. C. 2006, A&A Rev., 13, 31

Kumar, S.; Broadfoot, A. L., 1979, Astrophysical Journal, Part 1, vol. 228, Feb. 15, 1979, p. 302-311.

Kyrölä, E., Summanen, T., Schmidt, W., Mäkinen, T., Quémerais, E., Bertaux, J.-L., Lallement, R., & Costa, J. 1998, J. Geophys. Res., 103, 14523.

Lallement, R.; Bertaux, J. L.; Kurt, V. G., 1985; Journal of Geophysical Research (ISSN 0148-0227), vol. 90, Feb. 1, 1985, p. 1413-1423.

Lallement, R., Holzer, T. E., & Munro, R. H. 1985, J. Geophys. Res., 91, 6751

Lallement, R.; Raymond, J. C.; Bertaux, J.-L.; Quémerais, E.; Ko, Y.-K.; Uzzo, M.; McMullin, D.; Rucinski, D. 2004; Astronomy and Astrophysics, v.426, p.867-874.

Lamy, P.L. et al., *ESA SP*-**404**, 491-494, 1997.

Lamy, P.; Llebaria, A.; Quemerais, E., Advances in Space Research, Volume 29, Issue 3, p. 373-378, 2002.

Llebaria, A., Lamy, P.L., Koutchmy, S., *ESA SP*-**446**, 441-446, 1999.

Munro, R. H., & Jackson, B. V., 1977, ApJ, 213, 874

Pryor, W. R.; Barth, C. A.; Hord, C. W.; Stewart, A. I. F.; Simmons, K. E.; Gebben, J. J.; McClintock, W. E.; Lineaweaver, S.; Ajello, J. M.; Tobiska, W. K., 1996; Geophysical Research Letters, Volume 23, Issue 15, p. 1893-1896.

Quémerais, E.; Lamy, P., 2002, Astronomy and Astrophysics, v.393, p.295-304.

Quémerais, E.; Lallement, R.; Ferron, S.; Koutroumpa, D.; Bertaux, J.L.; Kyrölä, E.; Schmidt, W., 2006, J. Geophys. Res., Volume 111, Issue A9, CiteID A09114

Raymond, John C.; Fineschi, S.; Smith, P. L.; Gardner, L.; O'Neal, R.; Ciaravella, A.; Kohl, J. L.; Marsden, B.; Williams, G. V.; Benna, C.; et al.; 1998; ApJ, Volume 508, Issue 1, pp. 410-417.

Rucinski, D.; Fahr, H.J.; 1991; Annales Geophysicae (ISSN 0939-4176), vol. 9, Feb. 1991, p. 102-110.

Strachan, L., Panasyuk, A. V., Dobrzycka, D., Kohl, J. L., Noci G., Gibson, S.E. & Biesecker, D.A., 2000, J. Geophys. Res., vol 105, A2, 2345-2356.

Strachan, L., Suleiman, R., Panasyuk, A. V., Biesecker, D. A., & Kohl, J. L. 2002, ApJ, 571, 1008

Thomas G.E.; Krassa R.F.; 1971, Astronomy & Astrophysics, 11, 218.

Witt, N.; Blum, P. W.; Ajello, J. M., 1979; Astronomy and Astrophysics, vol. 73, no. 3, Mar. 1979, p. 272-281.

Woods, Thomas N.; Tobiska, W. Kent; Rottman, Gary J.; Worden, John R., 2000; Journal of Geophysical Research, Volume 105, Issue A12, p. 27195-27216.

Zouganelis, I., Meyer-Vernet, N., Landi, S., Maksimovic, M., & Pantellini, F. 2005, ApJ, 626, L117
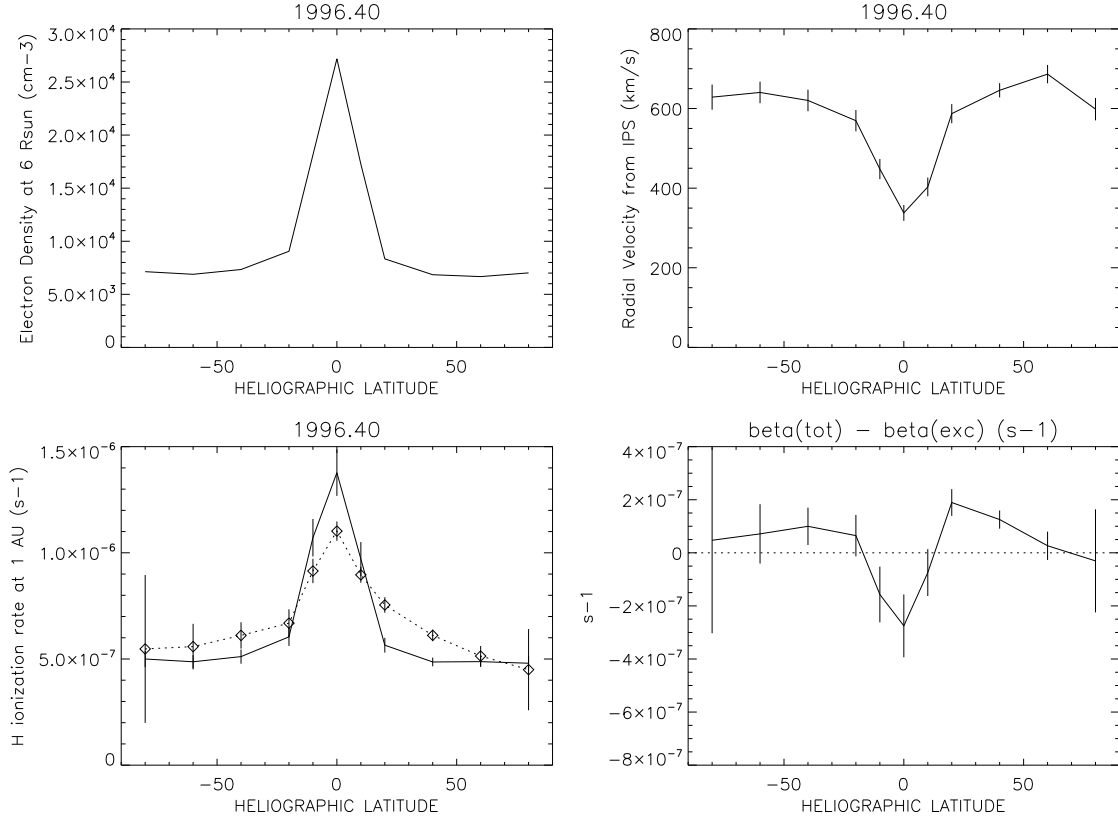
Fig. 1.— Monthly averages of the data used in this analysis. These values were obtained in March and April 1996. For all panels, the x axis shows the heliographic latitude. The top left panel shows the electron density at $6R_\odot$ obtained from the LASCO-C2 polarized white light images. The density is strongly enhanced around the equatorial belt. The top right panel shows the average solar wind velocity as deduced from the interplanetary scintillation data. We clearly see the fast wind at high latitudes and the slow wind around the equator. The bottom left panel shows the ionization rate of hydrogen at 1 AU. The diamonds joined by a dotted line shows the values derived from the SWAN data. The solid line shows the charge exchange ionization found when using the densities (scaled at 1 AU) and the velocities displayed in the top panels. The bottom right shows the difference between the SWAN values and the values obtained by combining the LASCO-C2 and IPS data. Note the excess produced by the SWAN values at high latitudes, i.e., for the fast solar wind.
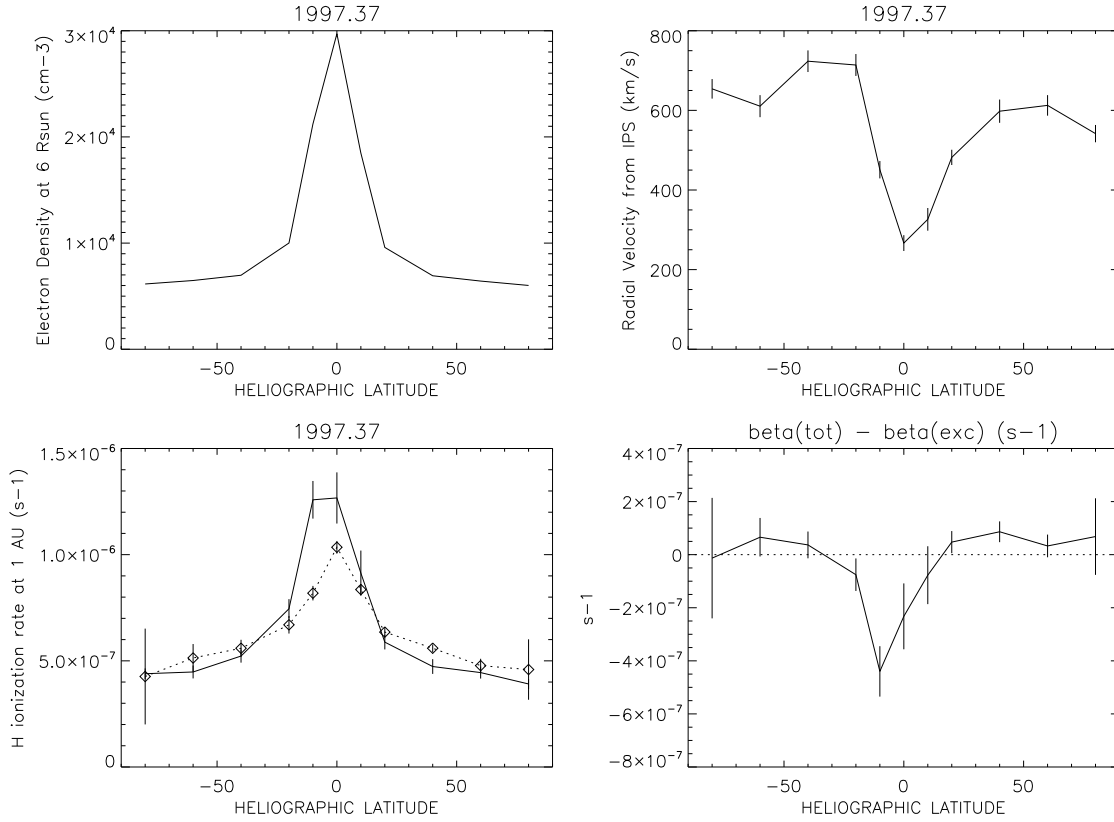
Fig. 2.— Same as the previous figure but for data obtained in Spring 1997. Although the numerical values are not identical, we find the same dichotomy between fast wind and slow wind. As shown in the bottom right panel, the flux deduced from the IPS values and and the LASCO-C2 data is too high along the equator. This means that the slow wind has not reached its terminal velocity at $6R_\odot$.
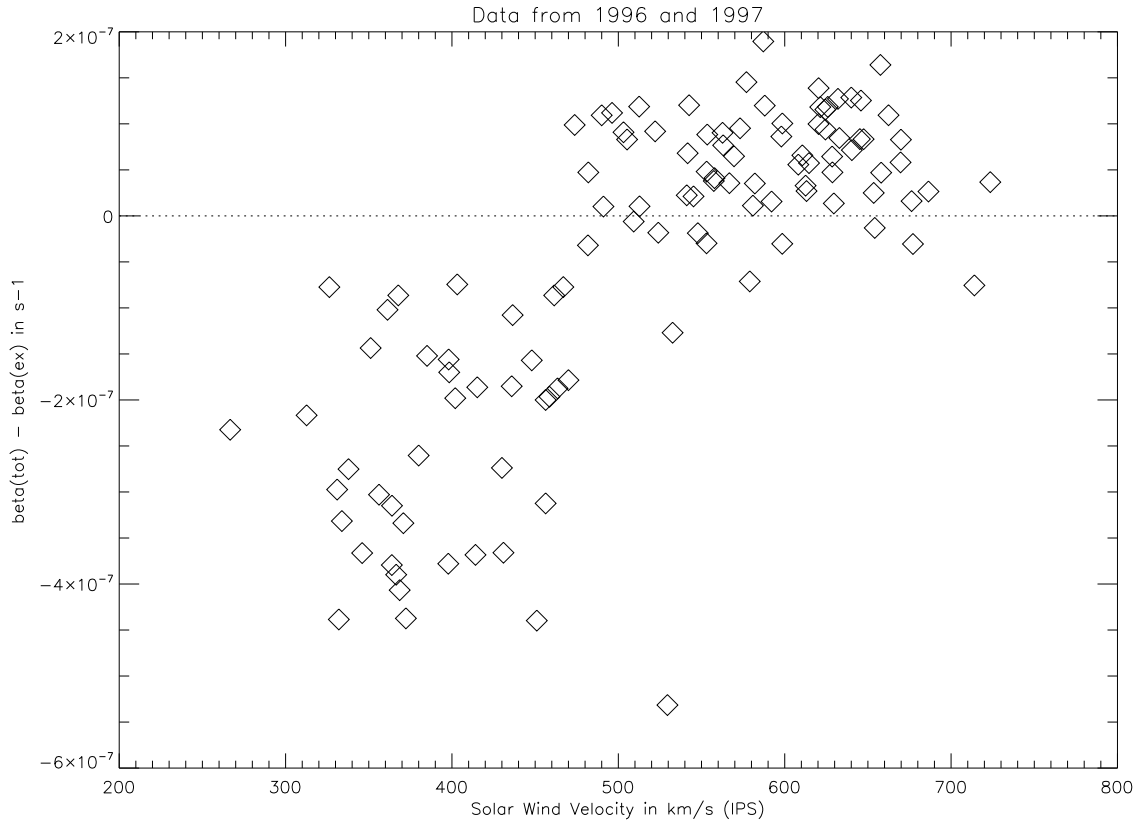
Fig. 3.— Difference between the SWAN total ionization rate at 1 AU and the charge exchange rate deduced from LASCO density and IPS velocity data. The x-axis shows the velocity value from the IPS data. In this plot, we have used all available data from 1996 and 1997, averaged monthly. The latitude bins are 10 degrees wide. Here we see the two types of wind. The fast wind (≥ 500 km/s) where the difference is positive and the slow wind where it is negative. The average of the fast wind values give an estimate for the sum of photo-ionization and electron impact ionization rates.
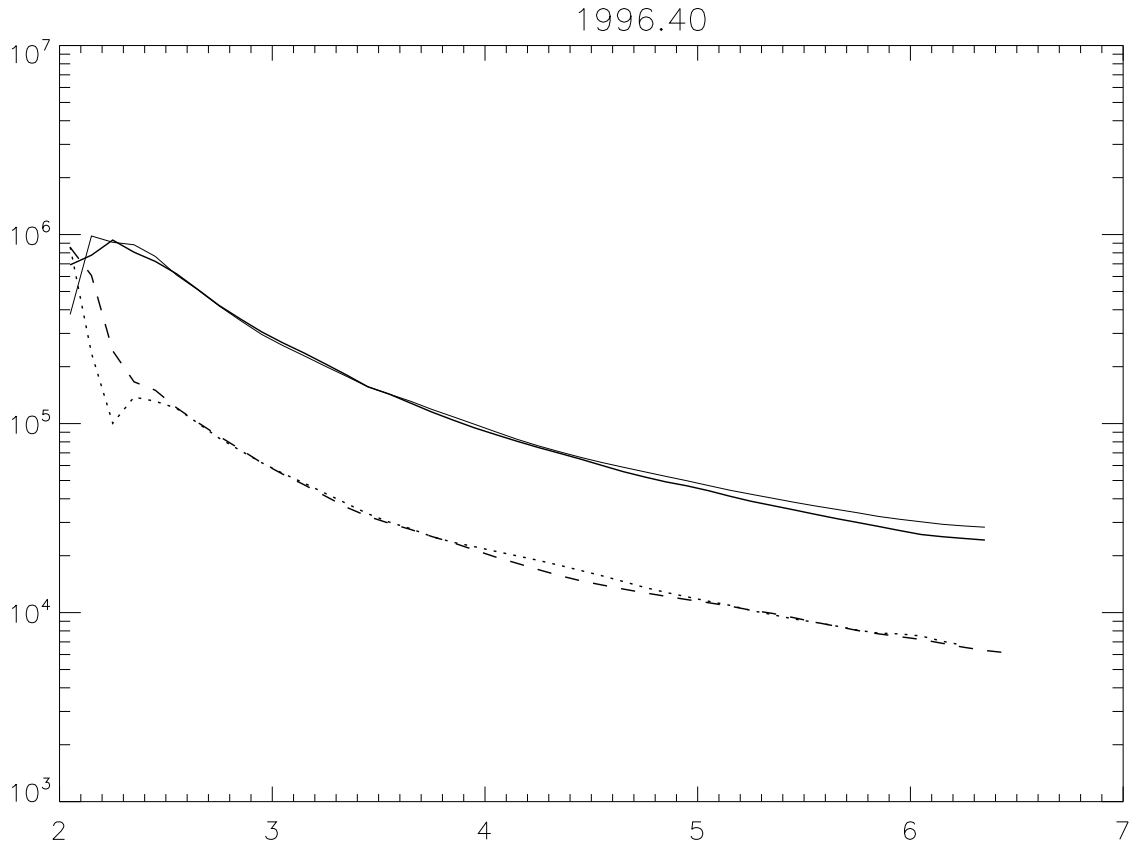
Fig. 4.— Density profiles for Spring 1996 deduced from the LASCO-C2 polarized white light images. The values correspond to one-month averages. The top solid lines give the values for the East and West limbs. The two limbs are very similar which is normal for an average of one month of data. The dashed line shows the north pole density profile and the dotted line shows the south pole profile. There's almost a factor of 10 between polar and equatorial values.
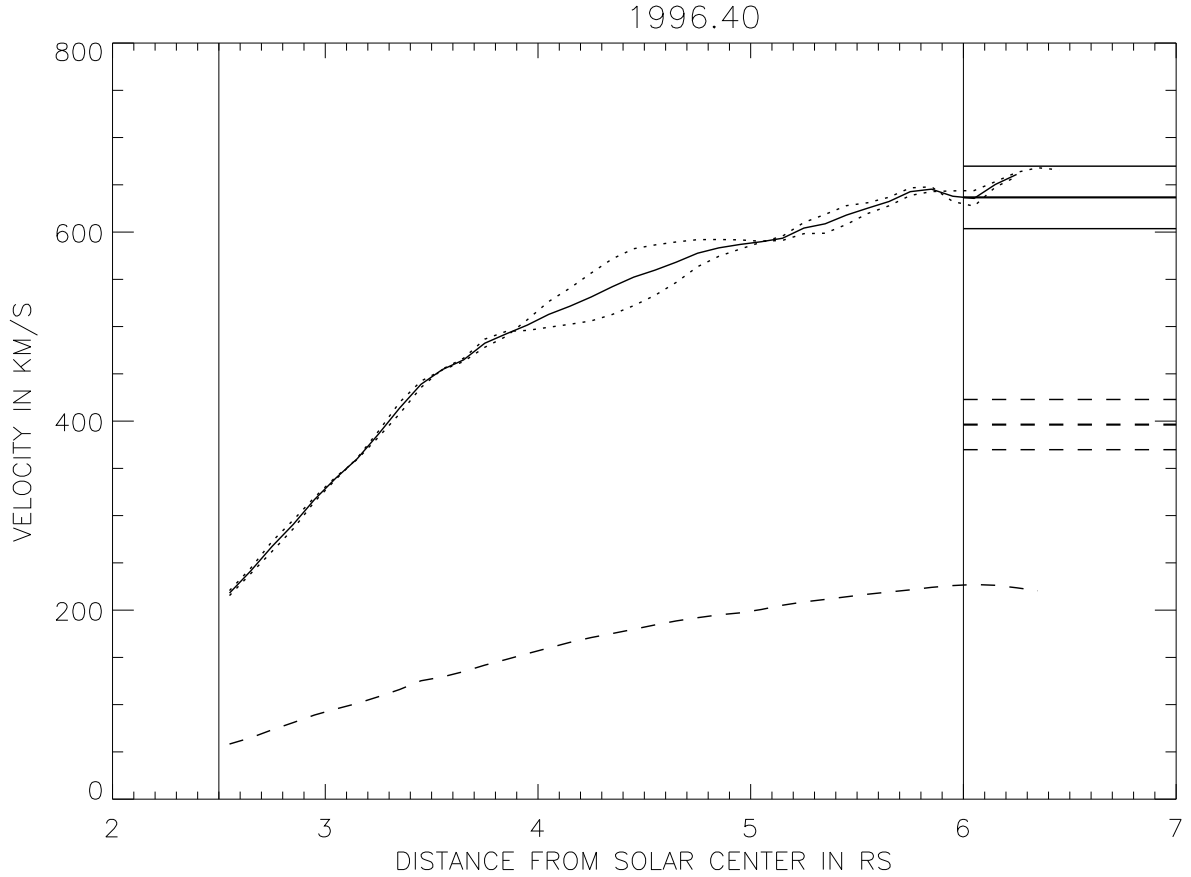
Fig. 5.— Velocity profiles for Spring 1996 deduced from the combination of SWAN, LASCO and IPS data. The solid line represents the average of the north and south profiles while the dotted lines show the individual north and south profiles. We see an inflexion around $3.5R_\odot$ which suggests a change in the acceleration at this altitude. The dashed line shows the profile derived for the equatorial solar wind. This profile was derived by assuming a radial expansion and may have to be corrected for non-radial effects. After $6R_\odot$, the lines show the IPS velocity values. For both polar profiles, we see that the profiles reach the terminal value around $6R_\odot$, whereas at the equator the velocity at $6R_\odot$ is only half of its terminal value.